REPORT

TOPOLOGICAL OPTICS

Generating arbitrary topological windings of a non-Hermitian band

Kai Wang*, Avik Dutt*, Ki Youl Yang, Casey C. Wojcik, Jelena Vučković, Shanhui Fan†

The nontrivial topological features in the energy band of non-Hermitian systems provide promising pathways to achieve robust physical behaviors in classical or quantum open systems. A key topological feature of non-Hermitian systems is the nontrivial winding of the energy band in the complex energy plane. We provide experimental demonstrations of such nontrivial winding by implementing non-Hermitian lattice Hamiltonians along a frequency synthetic dimension formed in a ring resonator undergoing simultaneous phase and amplitude modulations, and by directly characterizing the complex band structures. Moreover, we show that the topological winding can be controlled by changing the modulation waveform. Our results allow for the synthesis and characterization of topologically nontrivial phases in nonconservative systems.

The discoveries of a wide variety of topological materials, such as topological insulators (*1*, *2*) and Weyl semimetals (*3*, *4*), highlight the importance of topological band theory, which seeks to develop fundamental understandings of topological properties of energy band structures. Early efforts on topological band theory have focused on Hermitian Hamiltonians (*5*). Motivated in part by the developments in topological photonics (*6*), where gain and/or loss are common features (*7*–*9*), there have been emerging interests in developing topological band theory for non-Hermitian Hamiltonians (*10*–*12*).

The energy bands of non-Hermitian Hamiltonians exhibit nontrivial topological features that are absent in Hermitian systems. In particular, because the energy bands of non-Hermitian Hamiltonians are in general complex, generically even a single energy band in one dimension can form a nontrivial loop in the complex plane, as characterized by integer nonzero winding numbers (*11*, *12*). This is in contrast with Hermitian systems, where nontrivial topology requires at least two bands, and moreover requires symmetry protection in one dimension. Such nontrivial winding, which is specific to non-Hermitian systems, provides the topological underpinnings of notable phenomena such as the non-Hermitian skin effect (*13*, *14*) and necessitates the generalization of bulk-edge correspondence (*15*, *16*).

In spite of the central importance of energy band winding in the topological band theory of non-Hermitian systems, direct experimental observation and control of such winding have been lacking. Recent experiments have demonstrated the non-Hermitian skin effect (*13*, *15*, *17*) as well as the collapse of eigenspectrum as induced by the presence of an edge (*18*). These experiments, however, only provide indirect evidence of energy-band winding in non-Hermitian systems. Moreover, energy bands are defined only for infinite systems. For non-Hermitian systems, the eigenstates of a finite lattice can be qualitatively different from those in an infinite lattice. Thus,

Ginzton Laboratory and Department of Electrical Engineering, Stanford University, Stanford, CA 94305, USA.
*These authors contributed equally to this work.
†Corresponding author. Email: shanhui@stanford.edu

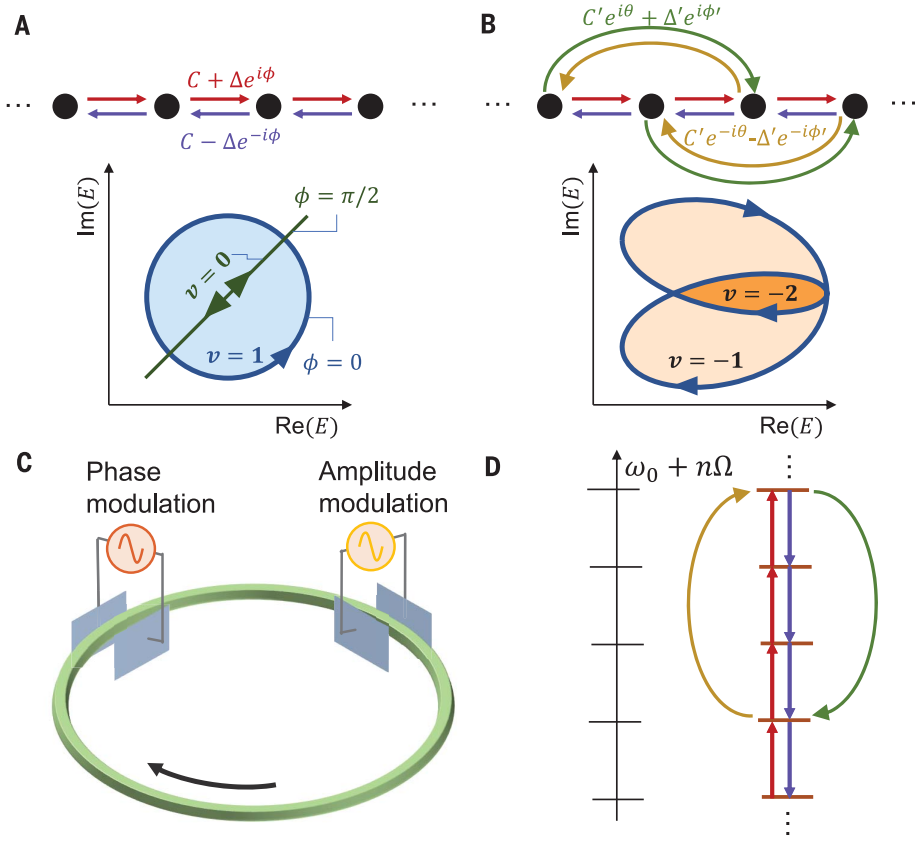

Fig. 1. Topological winding in a non-Hermitian 1D lattice and its realization in a synthetic frequency dimension. (**A**) A non-Hermitian 1D lattice with nearest-neighbor non-Hermitian coupling is shown at the top. The corresponding band energy winding in the complex plane, as k goes from 0 to 2π, is shown at the bottom. (**B**) Same as in (A) but with long-range coupling. A representative example of $v = -2$ is realized when a reference energy ϵ is in the inner dark orange–shaded region of the complex plane. (**C**) Realization of non-Hermitian 1D lattices using a ring resonator undergoing simultaneous amplitude and phase modulation at integer multiples of the free-spectral range Ω. (**D**) Frequency modes separated by Ω in the unmodulated resonator are presented on the left. Non-Hermitian coupling among the frequency modes created by both phase and amplitude modulation, shown for first- and third-order couplings as an illustrative example, are presented on the right.

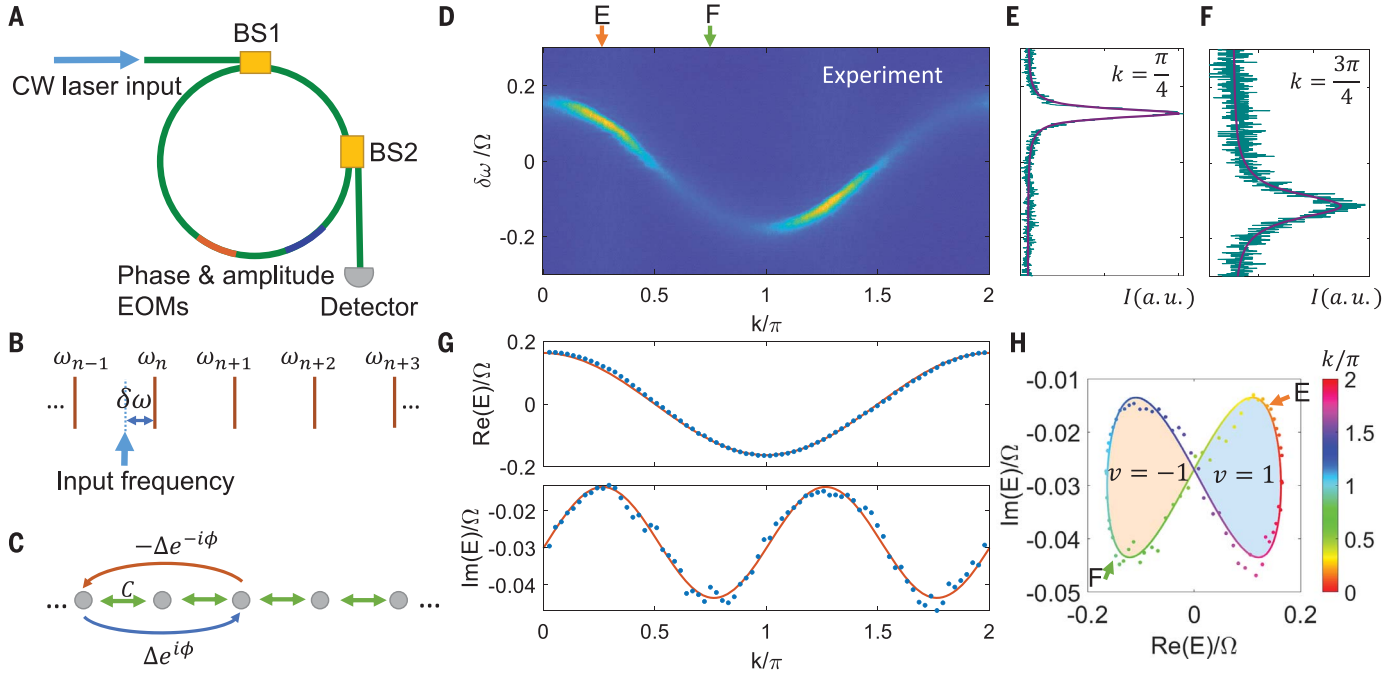

Fig. 2. Measurement of the *k*-resolved complex band energy in synthetic frequency space. (**A**) Input and output schematic of an optical fiber resonator simultaneously modulated by phase and amplitude EOMs. (**B**) A diagram of several resonant modes of the unmodulated resonator separated by Ω, where the input laser frequency (arrow) is detuned by δω from one of the resonance frequencies. (**C**) An example of the formed non-Hermitian lattice. (**D**) Color plot of experimentally measured output intensity $I(k, \delta\omega)$. (**E** and **F**) Measurement signal from two example vertical slices (teal curve) and Lorentzian fitting (purple curve) with (E) $k = \pi/4$ and (F) $k = 3\pi/4$. (**G**) Extracted *k*-dependent Re(*E*) and Im(*E*) (dots) from (D) compared with the theoretical prediction (curve). (**H**) The winding of the measured energy in the complex plane. Arrows indicate the corresponding points of the *k*-slices shown in (E) and (F).

it is not obvious how one can measure the band structure in experimentally feasible non-Hermitian lattices, which are typically finite.

We experimentally implement a class of non-Hermitian Hamiltonians and measure its momentum-resolved complex band energy. Our implementation uses the concept of a synthetic dimension (*19*–*22*), a synthetic frequency dimension (*23*–*25*) as formed by multiple frequency modes in a ring resonator under amplitude and phase modulations.

We implement in the frequency synthetic dimension the one-dimensional (1D) lattice Hamiltonian

$$\hat{H} = \sum_{m,n}\left(\kappa_{+m}\hat{a}^{\dagger}_{n+m}\hat{a}_n + \kappa_{-m}\hat{a}^{\dagger}_{n}\hat{a}_{n+m}\right) \quad (1)$$

where $\hat{a}^{\dagger}_n$ ($\hat{a}_n$) is the creation (annihilation) operator of the n-th lattice site with $m = 1, 2, \ldots, M$ running over the coupling orders. This Hamiltonian becomes non-Hermitian if $\kappa_{+m} \neq \kappa^{*}_{-m}$ for some m in Eq. 1. A general non-Hermitian form of the coupling constant $\kappa_{\pm m}$ can be given by $\kappa_{\pm m} = C_m\exp(\pm i\alpha_m) \pm \Delta_m\exp(\pm i\beta_m)$ with the coupling strengths $C_m, \Delta_m \geq 0$ and phases $\alpha_m, \beta_m \in (-\pi, \pi]$, where $C_m\exp(\pm i\alpha_m)$ is the Hermitian part and $\pm\Delta_m\exp(\pm i\beta_m)$ is the skew-Hermitian part. The Hamiltonian of Eq. 1 has been extensively explored theoretically (*11*, *26*); however, it has been challenging to implement such a Hamiltonian experimentally. The usual implementation of non-Hermitian Hamiltonians through the use of space-dependent gain and loss (*7*, *8*, *27*) does not straightforwardly create the non-Hermitian coupling in Eq. 1. Non-Hermitian couplings were only realized very recently on platforms that include pulse trains (*13*) and electronic circuits (*18*); these demonstrations, however, implemented only a limited subset of non-Hermitian coupling, i.e., nearest-neighbor coupling (exclusively $m = 1$) with restricted in-phase Hermitian and skew-Hermitian parts ($\alpha_1 = \beta_1$). It remains an open question if one can realize general non-Hermitian couplings, which include a control over coupling strengths (C_m, Δ_m), phases (α_m, β_m), and long coupling ranges ($m > 1$) (*23*, *24*, *28*). Our results illustrate the potential of the platform of synthetic dimensions to explore non-Hermitian topological physics and to implement Hamiltonians that are difficult to achieve by other means.

The Hamiltonian of Eq. 1 exhibits a rich set of nontrivial topological behaviors that depend on the strength, phase, and range of the coupling. We first consider the case with only nearest-neighbor coupling, where the only nonzero coupling constants are $\kappa_{-1} = C - \Delta\exp(-i\phi)$ and $\kappa_{+1} = C + \Delta\exp(i\phi)$ with C, $\Delta \geq 0$. The special case with $\phi = 0$ gives rise to the Hatano-Nelson model (*26*), where the band winds along an ellipse in the complex plane (Fig. 1A, bottom). For a reference energy $\epsilon \in \mathbb{C}$, a winding number (v) of such a 1D band can be defined by (*11*, *14*)

$$v := \int_0^{2\pi}\frac{\mathrm{d}k}{2\pi i}\frac{\mathrm{d}}{\mathrm{d}k}\ln\left[E(k) - \epsilon\right] \quad (2)$$

For the Hatano-Nelson model (Fig. 1A), if the reference energy ϵ is in the interior of the winding loop, e.g., in the shaded area of Fig. 1A, bottom, one obtains $v = 1$. We note that such a nontrivial winding is a topological feature that is specific to non-Hermitian Hamiltonians. For a Hermitian Hamiltonian, $E(k)$ is restricted to the real axis, and $v = 0$. We also note that the phase difference ϕ between the Hermitian and skew-Hermitian parts of the coupling strongly influences the shape of the loop. In the special example of $\phi = \pi/2$, $E(k)$ is restricted to a line and hence $v = 0$ (green line in Fig. 1A, bottom). More complex winding of the band structure can be achieved by introducing long-range coupling. As an example, we consider the case with $C = 0$, $\Delta/C' = \Delta'/C' = 1$, $\phi = \pi$, $\theta = 0$, and $\phi' = \pi$, where $v = -2$ for a suitable choice of the reference energy (Fig. 1B). In general, the sign of v is determined by the handedness of the winding, and $|v|$ depends on how many times the reference point ϵ is enclosed by the loop in each orientation.

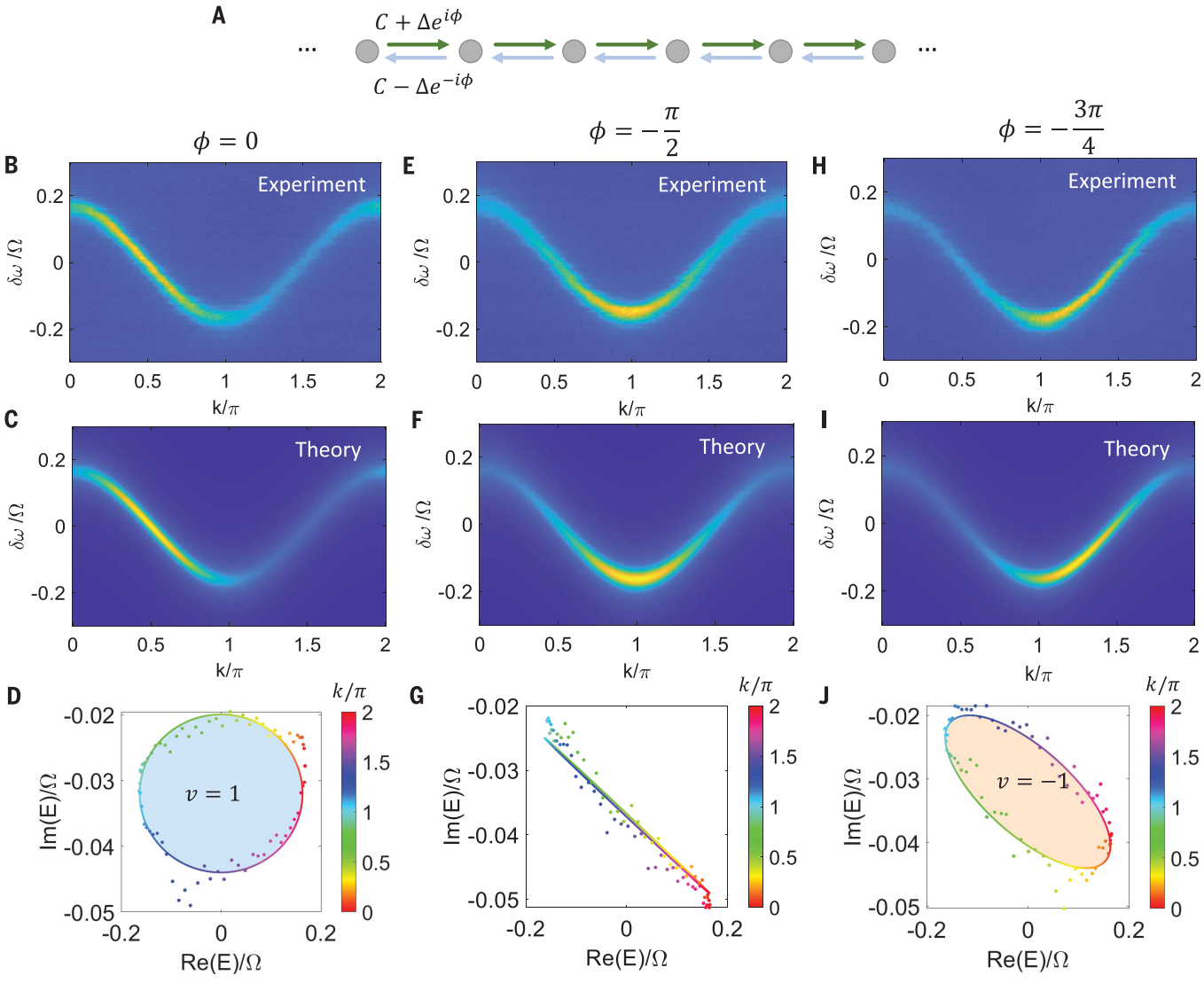

Fig. 3. Experimental realization of a generalized Hatano-Nelson model and the measured topological windings. (**A**) Lattice model with nearest-neighbor non-Hermitian couplings. (**B**, **E**, and **H**) Experimentally measured $I(k, \delta\omega)$ for ϕ = 0, −π/2, and −3π/4, respectively. (**C**, **F**, and **I**) Theoretical predictions for the measurements shown in (B), (E), and (H), respectively. (**D**, **G**, and **J**) The dots represent the band energy extracted from (B), (E), and (H), respectively. The lines denote theoretical predictions.

To experimentally realize the Hamiltonian of Eq. 1, we use the synthetic space as formed by the multiple frequency modes of a ring resonator. In the absence of modulation, the ring supports a set of resonant modes propagating along a specific direction (e.g., clockwise, as shown in Fig. 1C). These modes have frequencies $\omega_n = \omega_0 + n\Omega$, where n is an integer that indexes the mode. Ω is the free spectral range (FSR) (Fig. 1D, left). Hermitian coupling between nearest-neighbor frequency modes can be formed with the use of a phase modulation having an associated amplitude transmission factor $T_{\mathrm{Ph}} = \exp(-i\delta\Phi)$ with $\delta\Phi(t) = A_1\cos\Omega t$, where δΦ is the modulated phase, A_1 is the phase-modulation strength, and t is time. The strength of Hermitian coupling is $C \propto A_1$. Similarly, skew-Hermitian coupling can be formed with the use of an amplitude modulation having a transmission factor $T_{\mathrm{Am}} = 1 + B_1\sin(\Omega t + \phi)$, where B_1 is the modulation strength, because the amplitude modulation is not energy conserving. This gives rise to a skew-Hermitian coupling $\kappa_{\pm1} = \pm\Delta\exp(\pm i\phi)$ with the strength $\Delta \propto B_1$. With simultaneous phase and amplitude modulations, the model of Fig. 1A is realized. Longer-range coupling can be achieved with modulators having modulation frequencies $m\Omega$ with $m > 1$. Specifically, simultaneous implementation of the phase modulation $T_{\mathrm{Ph}} = \exp[-i\sum_m A_m\cos(m\Omega t + \alpha_m)]$ and the amplitude modulation $T_{\mathrm{Am}} = 1 + \sum_m B_m\sin(m\Omega t + \beta_m)$ will give rise to the Hamiltonian in Eq. 1, where $\kappa_{\pm m} = C_m\exp(\pm i\alpha_m) \pm \Delta_m\exp(\pm i\beta_m)$ [for more details, see supplementary section S1A (*29*)]. Consequently, this method allows for the realization of an arbitrary complex band structure for such one-band 1D non-Hermitian lattices, as illustrated in Fig. 1D, right, for a specific example. Note that the ability to simultaneously incorporate phase and amplitude modulations is essential for demonstrating topological winding. Hamiltonians with phase or amplitude modulation (*30*) alone do not exhibit nontrivial winding in their energy bands.

To directly measure the k-resolved non-Hermitian band structure in synthetic frequency space, we use a fiber ring resonator undergoing both phase and amplitude modulations by electro-optic modulators (EOMs) (Fig. 2A). We excite the system with a tunable continuous-wave (CW) laser via a beam splitter

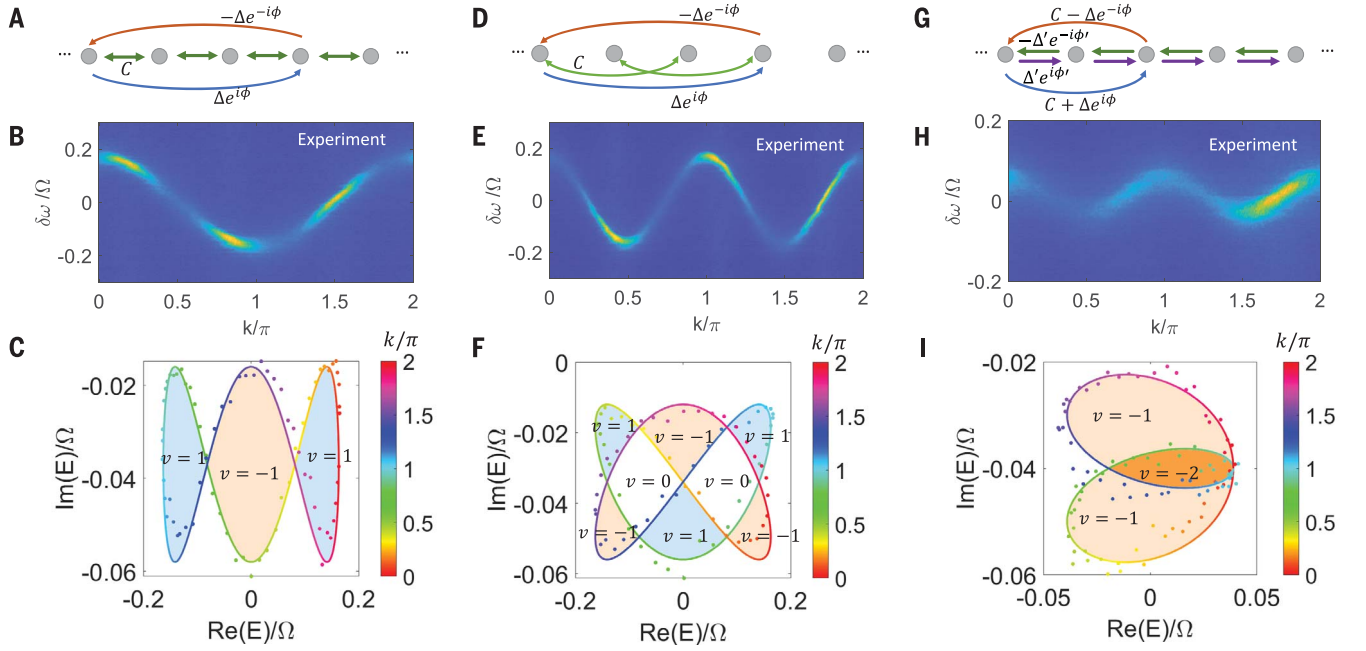

Fig. 4. Realization and band-winding measurements of non-Hermitian lattices incorporating long-range interactions. (**A**) A lattice with first-order Hermitian coupling and third-order skew-Hermitian coupling. (**D**) A lattice with second-order Hermitian coupling and third-order skew-Hermitian coupling. (**G**) A lattice with first-order skew-Hermitian coupling and second-order non-Hermitian coupling. (**B**, **E**, and **H**) Measured $I(k, \delta\omega)$ for the lattices in (A), (D), and (G), respectively. (**C**, **F**, and **I**) Deduced complex E in complex plane for the lattices in (A), (D), and (G), respectively. The dots are from experiments, and the lines are from theory.

(BS1). We choose the input laser frequency ω to be near a certain resonance ω_n, and sweep the detuning $\delta\omega = \omega_n - \omega$ (Fig. 2B). For each detuning, we allow the system to reach steady state and then measure the output from a second beam splitter (BS2) that samples a small portion of the intracavity light for time-resolved detection [for more details on the experimental setup, see supplementary section S2 (*29*)]. Because the lattice space is formed by frequency modes, its reciprocal space is inherently time t (*24*), with a round-trip time equivalent to one Brillouin zone; hence, we can define $k = t\Omega$ as the quasimomentum. The steady state resulting from our excitation contains all k components at that detuning δω. As we measure the output light at time $t = k/\Omega$, the detection selects a single k. Thus, the detected signal $I(k, \delta\omega)$ can be understood as the steady state projected to the discrete Bloch state $|k\rangle$. $I(k, \delta\omega)$ is related to the Green's function, $G(k, \delta\omega) = i[\delta\omega - E(k)]^{-1}$, as

$$I(k,\delta\omega) \propto |G(k,\delta\omega)|^2 = \frac{1}{[\mathrm{Re}(E)-\delta\omega]^2 + [\mathrm{Im}(E)]^2} \quad (3)$$

Here, the band energy is

$$E(k) = \langle k|\hat{H} - i\gamma|k\rangle \quad (4)$$

where γ denotes all sources of loss in the absence of modulation. For a given k, I is a Lorentzian function of δω. Then, at each k, it is possible to deduce the values of Re(E) and |Im(E)| by fitting $I(\delta\omega)$ to the form of Eq. 3. In our setup, we use a cavity with a sufficiently large loss, i.e., a sufficiently large positive $\gamma \approx 2\Delta + 0.02\Omega$, such that Im($E$) < 0 is ensured for all k. For a γ that is independent of k, $E(k)$ differs from the dispersion of $\hat{H}$ by a translation in the complex energy plane. The topological properties are not affected by such a translation.

To illustrate the specific process of the band-structure measurement, we show a representative experiment forming a lattice in synthetic frequency space (Fig. 2C). There is a first-order Hermitian coupling $\kappa_{\pm 1} = C$ and a second-order skew-Hermitian coupling $\kappa_{\pm 2} = \pm\Delta\exp(\pm i\phi)$. By scanning k over one Brillouin zone and δω over one FSR Ω, we obtain the $I(k, \delta\omega)$ readouts (Fig. 2D). Here, we show two representative slices of $I(\delta\omega)$ at $k = \pi/4$ and $k = 3\pi/4$ (Fig. 2, E and F, respectively). According to Eq. 3, Re(E) and Im(E) can be obtained by a Lorentzian fit for each k-slice of I (purple curves in Fig. 2, E and F). We plot Re(E) and Im(E) that are thus obtained as the dots in Fig. 2G. The red curves in Fig. 2G indicate the theoretically predicted form of the dispersion, which agrees well with the experimentally measured dots. Finally, we plot E in the complex plane and visualize the winding (Fig. 2H). For the specific dispersion in this example, the complex band winds into a bow-tie shape. For k going from 0 to 2π, the left-side loop (light orange shading) is traversed clockwise once with the winding number v = −1, and the right-side counterclockwise loop (light blue shading) has v = 1.

Band structures are only defined for infinite systems that fulfill Bloch's theorem, whereas all practical structures in experiments are finite. Thus, in seeking to experimentally measure a band structure, one is always attempting to infer the property of an infinite system through the measurement on a corresponding finite system. For the Hermitian system, this does not present an issue. Within the energy range of the band in an infinite system, the eigenstates of the corresponding finite system are also extended and provide an increasingly better approximation of the eigenstates of the infinite system as the size of the finite system increases. For the non-Hermitian system, on the other hand, the eigenstates of the finite system can be drastically different from those of the infinite system. As an extreme example, a finite non-Hermitian lattice truncated with an open boundary condition (OBC) can exhibit the non-Hermitian skin effect with all eigenstates localized on the edge, and the eigenspectra are thus completely different from those of the corresponding infinite system (*14*, *18*). Thus, it was noted that the winding number defined in Eq. 2 cannot be simply identified from the eigenspectrum of a finite non-Hermitian system (*11*). And hence it may appear surprising that through Eq. 3 we are able to measure the band structure of an infinite system by experiments on a finite system. We emphasize that our experiments probe $E(k)$ as defined by Eq. 4. $E(k)$

is not an eigenenergy of the finite system but rather the expectation value of the Hamiltonian of the finite system at state $|k\rangle$. The state $|k\rangle$ is always extended and moreover naturally approaches the Bloch state of an infinite system as the system size increases. Consequently, our experiments can provide a measurement of the band structure of an infinite system satisfying Bloch's theorem. As an illustration, in supplementary section S1B and fig. S1 (*29*) we consider a numerical experiment where we apply our technique for the extreme case as mentioned above where a finite non-Hermitian lattice is truncated by the OBC. Even though such a finite lattice exhibits a non-Hermitian skin effect, our technique still provides a faithful measurement of the band structure of the infinite system.

We now present an example where the winding of the band can be straightforwardly controlled. In Fig. 3A, we sketch a lattice with nearest-neighbor non-Hermitian couplings in the form $\kappa_{\pm1} = C \pm \Delta\exp(\pm i\phi)$. Importantly, the topological winding is largely determined by the value of the phase ϕ, which can readily be tuned in our experiments by varying the relative phase between the amplitude and phase modulations. Figure 3, B and C, shows the band structure measurement for $\phi = 0$ accompanied by a theoretical prediction. This case serves as a faithful realization of the Hatano-Nelson model (*26*). The complex band encircles an elliptical area in the counterclockwise direction (Fig. 3D) corresponding to a winding number $v = 1$ (light blue shading). By contrast, if we have $\phi = -\pi/2$ (Fig. 3, E and F), the topology is trivial—the band forms a line in the complex plane (Fig. 3G). As we further choose $\phi = -3\pi/4$ (Fig. 3, H and I), the band becomes a tilted ellipse with a clockwise handedness (Fig. 3J). The winding number with respect to a reference energy inside the loop becomes $v = -1$.

A strength of the synthetic-dimension approach lies in the ability to readily incorporate long-range couplings, which can also be non-Hermitian. We harness this ability to produce more complex windings. In Fig. 4A, we sketch a lattice model with a Hermitian first-order coupling $\kappa_{\pm1} = C$ and a skew-Hermitian third-order coupling $\kappa_{\pm3} = \pm\Delta\exp(\pm i\phi)$. This lattice has a dispersion $E(k) = 2C\cos(k) + 2i\Delta\sin(3k + \phi) - i\gamma$. Figure 4, B and C, shows the measurement results for $\phi = 0$. The extracted complex band winding is shown in Fig. 4C, which encloses three areas with the winding number $v = 1$, -1, and 1 from left to right, respectively. As another example, in Fig. 4D, the Hermitian coupling is varied to second order compared with the lattice in Fig. 4A, and hence the dispersion becomes $E(k) = 2C\cos(2k) + 2i\Delta\sin(3k + \phi) - i\gamma$. We show a measurement and the extracted complex band winding with $\phi = -3\pi/4$ (Fig. 4, E and F, respectively). The winding loop encloses three areas with $v = 1$ (light blue shading), three areas with $v = -1$ (light orange shading), and two areas with $v = 0$ (no shading). These examples act as longer-range generalizations of the instances shown in Fig. 3. Additionally, because the winding number v theoretically can take any integer value, to showcase the capability of implementing and measuring windings with $|v| > 1$, we also present an instance as shown in Fig. 4, G to I. The lattice model illustrated in Fig. 4G incorporates non-Hermitian couplings of both first and second orders, where we have $\kappa_{\pm1} = \pm\Delta'\exp(\pm i\phi')$, $\kappa_{\pm2} = C \pm \Delta\exp(\pm i\phi)$. The Bloch band is given by $E(k) = 2C\cos(2k) + 2i\Delta'\sin(k + \phi') + 2i\Delta\sin(2k + \phi) - i\gamma$. In Fig. 4H, we show the measurement for the case $\phi = \phi' = \pi$, and the winding loop encloses not only areas with $v = -1$ (light orange shading) but also an area that winds twice clockwise, which corresponds to $v = -2$ (dark orange shading). In this example, we use a different phase modulation strength that alters the range of $\mathrm{Re}(E)$ (Fig. 4I; see also fig. S7). More examples of experimental results can be found in supplementary section S3 (*29*).

Our experimental observation of topological windings of the complex band energy shows that non-Hermitian lattice Hamiltonians in the frequency synthetic space can be implemented through simultaneous amplitude and phase modulations of a ring resonator supporting multiple resonant modes. The realization of non-Hermitian lattice Hamiltonians in synthetic space brings unprecedented flexibility to arbitrarily tailor the complex band structure, fully combining non-Hermitian, long-range, and complex-valued couplings. Such an experimental platform holds great promise in the exploration of highly complex behaviors in synthetic frequency space, such as the interplay of gain, loss, topology, dimensionality, nonlinearity, and lasing.

REFERENCES AND NOTES

1. C. L. Kane, E. J. Mele, *Phys. Rev. Lett.* **95**, 146802 (2005).
2. M. König *et al.*, *Science* **318**, 766–770 (2007).
3. L. Lu *et al.*, *Science* **349**, 622–624 (2015).
4. S.-Y. Xu *et al.*, *Science* **349**, 613–617 (2015).
5. X.-L. Qi, S.-C. Zhang, *Rev. Mod. Phys.* **83**, 1057–1110 (2011).
6. T. Ozawa *et al.*, *Rev. Mod. Phys.* **91**, 015006 (2019).
7. M. A. Bandres *et al.*, *Science* **359**, eaar4005 (2018).
8. H. Zhao *et al.*, *Science* **365**, 1163–1166 (2019).
9. B. Bahari *et al.*, *Science* **358**, 636–640 (2017).
10. H. Shen, B. Zhen, L. Fu, *Phys. Rev. Lett.* **120**, 146402 (2018).
11. Z. Gong *et al.*, *Phys. Rev. X* **8**, 031079 (2018).
12. C. C. Wojcik, X.-Q. Sun, T. Bzdušek, S. Fan, *Phys. Rev. B* **101**, 205417 (2020).
13. S. Weidemann *et al.*, *Science* **368**, 311–314 (2020).
14. N. Okuma, K. Kawabata, K. Shiozaki, M. Sato, *Phys. Rev. Lett.* **124**, 086801 (2020).
15. L. Xiao *et al.*, *Nat. Phys.* **16**, 761–766 (2020).
16. S. Yao, Z. Wang, *Phys. Rev. Lett.* **121**, 086803 (2018).
17. A. Ghatak, M. Brandenbourger, J. van Wezel, C. Coulais, *Proc. Natl. Acad. Sci. U.S.A.* **117**, 29561–29568 (2020).
18. T. Helbig *et al.*, *Nat. Phys.* **16**, 747–750 (2020).
19. O. Boada, A. Celi, J. I. Latorre, M. Lewenstein, *Phys. Rev. Lett.* **108**, 133001 (2012).
20. L. Yuan, Q. Lin, M. Xiao, S. Fan, *Optica* **5**, 1396 (2018).
21. T. Ozawa, H. M. Price, *Nat. Rev. Phys.* **1**, 349–357 (2019).
22. E. Lustig *et al.*, *Nature* **567**, 356–360 (2019).
23. B. A. Bell *et al.*, *Optica* **4**, 1433 (2017).
24. A. Dutt *et al.*, *Nat. Commun.* **10**, 3122 (2019).
25. A. Dutt *et al.*, *Science* **367**, 59–64 (2020).
26. N. Hatano, D. R. Nelson, *Phys. Rev. Lett.* **77**, 570–573 (1996).
27. M. Wimmer, M.-A. Miri, D. Christodoulides, U. Peschel, *Sci. Rep.* **5**, 17760 (2015).
28. A. González-Tudela, C.-L. Hung, D. E. Chang, J. I. Cirac, H. J. Kimble, *Nat. Photonics* **9**, 320–325 (2015).
29. See supplementary materials.
30. L. Yuan, Q. Lin, M. Xiao, A. Dutt, S. Fan, *APL Photonics* **3**, 086103 (2018).

ACKNOWLEDGMENTS

We acknowledge D. A. B. Miller for providing lab space and equipment and M. Orenstein for useful discussions. **Funding:** This work is supported by a MURI project from the U.S. Air Force Office of Scientific Research (grant no. FA9550-18-1-0379) and by a Vannevar Bush Faculty Fellowship from the U.S. Department of Defense (grant no. N00014-17-1-3030). **Author contributions:** K.W., A.D., and S.F. initiated the idea; K.W. and A.D. developed the theory, with input from C.C.W.; K.W. and A.D. performed the experiments, with input from K.Y.Y. and J.V.; and K.W. and A.D. processed the data. All authors discussed the results and contributed to writing the manuscript. S.F. supervised the work. **Competing interests:** The authors declare no competing interests. **Data and materials availability:** All data needed to evaluate the conclusions in this study are presented in the paper and in the supplementary materials.

SUPPLEMENTARY MATERIALS

science.sciencemag.org/content/371/6535/1240/suppl/DC1
Materials and Methods
Figs. S1 to S7
References (*31*–*45*)

10 November 2020; accepted 9 February 2021
10.1126/science.abf6568

Generating arbitrary topological windings of a non-Hermitian band

Kai Wang, Avik Dutt, Ki Youl Yang, Casey C. Wojcik, Jelena Vuckovic and Shanhui Fan

Science **371** (6535), 1240-1245.
DOI: 10.1126/science.abf6568

Topology in the open

Controlling the topology of a system provides a route to develop devices that are robust against defects. Whereas earlier developments of topological band theory focused on Hermitian (closed) systems, recent efforts have been toward non-Hermitian (open) systems. K. Wang *et al.* report on the measurement and control of topologically nontrivial windings of a non-Hermitian energy band. By implementing non-Hermitian lattice Hamiltonians along a frequency synthetic dimension formed by optical frequency modes in a modulated ring-resonator, they directly visualized the nontrivial topological band winding and showed that the winding can be controlled. Such control provides a route for the experimental synthesis, characterization, and control of topologically nontrivial phases in open physical systems.

Science, this issue p. 1240